

Optimization of $\leq 200\mu\text{m}$ pitch CZT detectors for future high-resolution X-ray instrumentation in astrophysics

Anna Zajczyk^a, Marie Draper^a, Paul Dowkontt^a, Qingzhen Guo^a, Fabian Kislat^a, Henric Krawczynski^a, Gianluigi De Geronimo^b, Shaorui Li^b, Matthias Beilicke^a

^aDepartment of Physics and McDonnell Center for Space Sciences, Washington University in St. Louis, 1 Brookings Drive, St. Louis, MO 63105, USA;

^bBrookhaven National Laboratory, Upton, NY 11973, USA;

ABSTRACT

Cadmium Zinc Telluride and Cadmium Telluride are the detector materials of choice for the detection of X-rays in the X-ray energy band $E \geq 5\text{ keV}$ with excellent spatial and spectral resolution and without cryogenic cooling. Owing to recent breakthroughs in grazing incidence mirror technology, next-generation hard X-ray telescopes will achieve angular resolution between 5 and 10 arc seconds - about an order of magnitude better than that of the NuSTAR hard X-ray telescope. As a consequence, the next generation of X-ray telescopes will require pixelated X-ray detectors with pixels on a grid with a lattice constant of $\leq 250\mu\text{m}$. Additional detector requirements include a low energy threshold of less than 5 keV and an energy resolution of less than one keV. The science drivers for a high angular-resolution X-ray mission include studies and measurements of black hole spins, the cosmic evolution of super-massive black holes, active galactic nuclei feedback, and the behaviour of matter at very high densities. In this contribution, we report on our R&D studies with the goal to optimise small-pixel Cadmium Zinc Telluride and Cadmium Telluride detectors.

Keywords: CdZnTe (CZT), CdTe, semiconductor detector, pixelization, performance, X-ray astronomy

1. INTRODUCTION

Owing to recent breakthroughs in grazing incidence mirror technology, next-generation X-ray telescopes will achieve angular resolution of 5 – 10 arc seconds.^{1,2} Such telescopes require pixelated detectors with a pixel-to-pixel pitch of $\leq 250\mu\text{m}$. A low energy threshold of $< 5\text{ keV}$ and an energy resolution of $< 1\text{ keV}$ are additional requirements for future X-ray satellite missions to enable spectroscopic studies of emission processes in the universe. The science drivers for a high angular-resolution X-ray mission include studies and measurements of black hole spins, the cosmic evolution of super-massive black holes, active galactic nuclei (AGN) feedback, and the behaviour of matter at very high densities.

A high stopping power, good spectral performance and good imaging capabilities are required from materials used as detectors in the X-ray energy band. Semiconductors like silicon (Si) and germanium (Ge) yield excellent energy resolution. However, due to its low density of 2.33 g cm^{-3} and low atomic number of 14, silicon is inefficient at stopping high energy photons, which limits its use to only low energies. At the same time, due to its small band gap germanium needs to be operated at cryogenic temperatures in order to decrease its dark current. Thus, semiconductors with high atomic number Z , high density ρ and wide band gap E_{gap} that meet the aforementioned requirements have been developed. Refer to Tab. 1 for comparison of properties of selected semiconductors.

Cadmium telluride (CdTe) and cadmium zinc telluride (CZT) crystals proved to be a well-suited material for detecting hard X-ray and soft γ -ray photons in astrophysical applications (e.g. Burst Alert Telescope⁵ on board the Swift satellite consists of 32,768 CZT detectors sensitive to photons in the energy range between 15 keV and 150 keV). Properties that make CdTe/CZT almost perfect X-ray detector materials are their high average atomic numbers ($Z_{\text{Cd}} = 48$, $Z_{\text{Te}} = 52$) and their high densities ($\rho_{\text{CdTe}} = 5.85\text{ g cm}^{-3}$, $\rho_{\text{CdZnTe}} = 5.81\text{ g cm}^{-3}$). The former causes photoelectric absorption to be a dominant photon-interaction process in the material up to

Further author information: (Send correspondence to A. Zajczyk): azajczyk@physics.wustl.edu

Table 1. Properties of selected semiconductors:³ density ρ , atomic number Z , band gap width E_{gap} , and intrinsic energy resolution ΔE_{intr} . The width of the band gap of CZT crystal increases with the increase of Zn concentration.⁴ The widely used composition of $\text{Cd}_{1-x}\text{Zn}_x\text{Te}$ has $x = 0.08 - 0.15$ resulting in the band gap of ~ 1.6 eV.

Semi-conductor	ρ [g cm ⁻³]	Z	E_{gap} [eV]	ΔE_{intr} [eV]
Si	2.33	14	1.12	450
Ge	5.33	32	0.67	400
CdTe	5.85	48, 52	1.44	700
CZT	5.81	48, 52	1.6-2.2	620

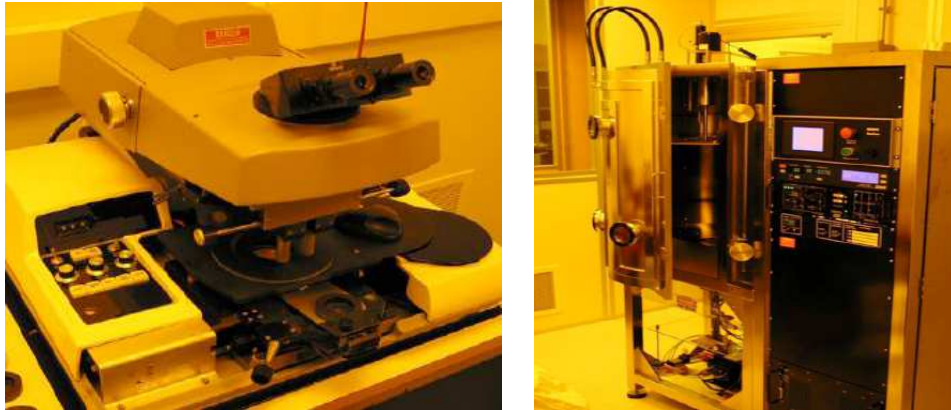


Figure 1. The class-100 clean room operated by our group (Physics Department at Washington University in St. Louis). **Left:** A photolithography station to prepare the pixel patterns to be deposited onto the detectors. **Right:** A vacuum electron-beam evaporator to deposit thin metal films and/or oxides onto the surface of a crystal.

about 300 keV. The latter results in a good photon stopping power. Moreover, a wide band gap of CdTe/CZT allows for operation at room temperature. Though not devoid of problems of their own,^{3,4} e.g. charge trapping or ballistic deficit, CdTe/CZT crystals have an intrinsic energy resolution* comparable to that of germanium. The presented properties of CdTe/CZT and our prior experience in fabrication of and signal processing from CZT detectors make these semiconductors our materials of choice for performance studies of fine-pitch $\leq 350 \mu\text{m}$ pixelated anodes for future high-resolution X-ray detectors.

Our semiconductor research group at the Physics Department of Washington University in St. Louis operates a class-100 clean room (Fig. 1), and we work on the development and optimization of pixelated CZT detectors. The detectors can be used in X-ray astronomy and in applications related to medical instrumentation. An example of an application of the CZT detectors in astrophysics is the recently developed X-ray scattering polarimeter X-Calibur which is discussed elsewhere.^{6,7}

This paper is structured as follows: the experimental setup and data analysis methods are described in Sec. 2, the results on the fine-pitch CZT detector and CdTe detectors are presented in Sec. 3, and the concluding remarks can be found in Sec. 4.

2. EXPERIMENTAL SETUP AND MEASUREMENTS

The goal of our study is to fabricate and characterise the performance of CZT and CdTe detectors with pixelated anodes of pixel size d in the range between $100 \mu\text{m}$ and $250 \mu\text{m}$ and pixel pitch p of $200 \mu\text{m} - 500 \mu\text{m}$. The detectors are characterized by their energy resolution, energy threshold and their detection efficiency as a function of energy. We also plan to study the charge sharing between pixels for different pixel pitches.

*Intrinsic energy resolution is the energy resolution derived from taking into account only statistical fluctuations of electron-hole pair creation.

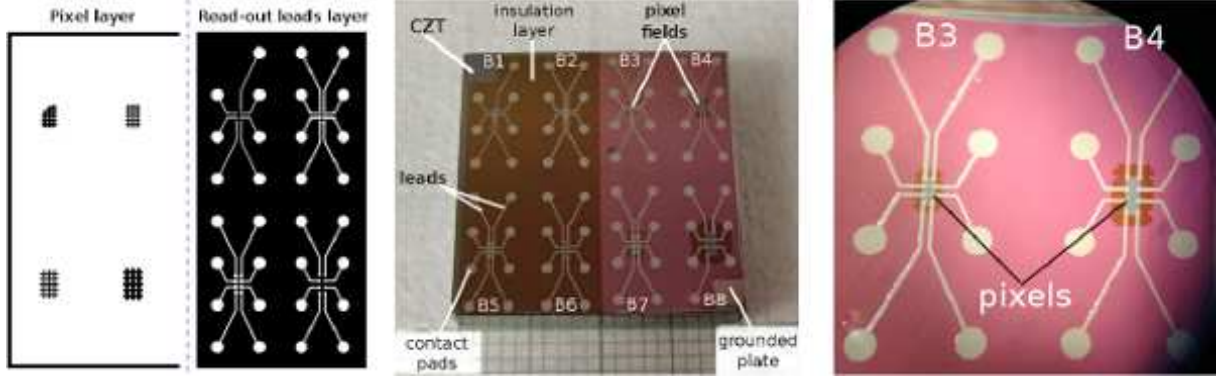


Figure 2. Photomask layout and fabricated detector with fine-pitch pixels. **Left:** view of selected layers from the fine-pitch pixel photomask. The left side shows the first layer with pixel blocks surrounded by the grounded plate. The right side depicts the third layer bearing leads and circular contact pads through which the signal is transported from individual pixels. **Middle:** image of the fabricated CZT detector. All eight pixel blocks are visible. Pixels and leads/contact pads show up in silver colour. The insulation layer is made of Al_2O_3 (brown/pink-coloured material). Different colouring of the insulation layer on the left side of the detector (for deposition testing purposes). **Right:** blow-up of the top right quarter of the detector (blocks B3 and B4). Clearly visible are pixel blocks consisting of 2×8 pixels. Pixels are surrounded by the grounded plate, whose edge is shaped in a way to mimic a continuation of the pixel grids. Narrow leads (width of $70 - 100 \mu\text{m}$) carry the signal from pixels to circular contact pads. The contact pads are spaced at a pitch of 2.4 mm to match our standard read-out detector fixture capable of reading out 8×8 pixels (see Sec. 2.2). Leads/pads are separated from the grounded plate by a layer of insulating Al_2O_3 (pink-coloured material).

2.1 Fine-pitch anode detector fabrication

A photomask with a fine-pitch anode layout was designed and fabricated (Fig. 2, left). The anode is comprised of eight pixel blocks, each with a different pixel size and pitch (see Tab. 2.1 for values of d and p for each pixel block). Each pixel block comprises up to eight small pixels. The signal from a pixel is transferred via a lead to a circular contact pad that is then connected to the read-out system. In the currently investigated design, the anode consists of three layers: 1) *pixel* layer with a grounded plate filling the space between the individual pixel blocks, 2) *insulation* layer, and 3) *read-out leads* layer. The *pixel* layer is the one deposited directly onto the detector surface, while the *read-out leads* layer is the topmost layer (on top of the *insulation* layer) in this sandwich-like design. In the standard setup of our read-out system, spring-loaded pogo pins (Fig. 3) are used to transfer the signal from detector pixels to ASIC (Application Specific Integrated Circuit) channels. However, we are also experimenting with a zebra pad (Fig. 4, top left) and gold wire bonds (Fig. 4, top right) as alternative methods of signal transfer from small-sized pixels to ASIC channels.

The detector's anode was fabricated in our class-100 clean room. The fabrication was performed in three stages: 1) pixel layer, 2) insulation layer and 3) read-out leads layer application. Each stage consisted of a photolithography processing followed by the deposition of a metal (layer 1 and 3) or an insulator (layer 2) film with an electron beam physical vapour deposition system. The steps in the photolithography process included: pre-baking, applying Microposit S1813 positive photoresist, post-baking, mask alignment, UV exposure, development in Microposit CD-30 Developer, and removing the remaining photoresist with Microposit Remover 1165 after a thin film evaporation. The detector surface was polished and etched with Bromine solution (5% Bromine, 95% Methanol) before carrying out the photolithography and thin film deposition steps of stage one. More details on the detector preparation and fabrication can be found in Li et al. (2011).⁸ Titanium was used as a material for the pixel/grounded plate layer. Aluminium oxide Al_2O_3 was used as an insulation material. The fabricated anode on a CZT crystal is presented in the middle/right panels of Fig. 2. The insulation layer of aluminium oxide is $\sim 2 \text{ k}\text{\AA}$ thick, while the pixels/grounded plate and the leads/contact pads are $\sim 1.25 \text{ k}\text{\AA}$ and $\sim 3 \text{ k}\text{\AA}$ thick, respectively. The CZT detector used in our study has a monolithic gold cathode. The design/fabrication of multiple pixel blocks has the advantage to simultaneously test different pixel geometries on the same detector

Table 2. Parameters of pixel blocks B of the fine-pitch pixelated anode (see Fig. 2 for the positions of the blocks B1 to B8). Along the values of pixel size d and pixel pitch p , the number of pixels in each block is given.

Block name	d [μm]	p [μm]	No. pixels
B1	100	250	7
B2	150	250	8
B3	100	200	8
B4	100	300	8
B5	200	300	8
B6	150	350	8
B7	250	350	8
B8	150	500	7

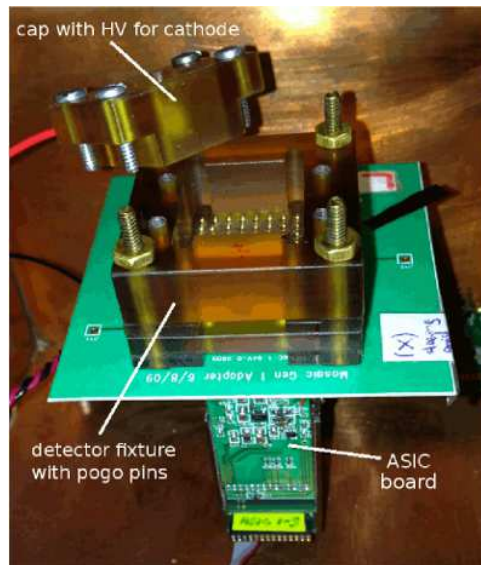


Figure 3. The detector read-out system. Shown here is the adapter board (designed at Washington University) with the detector fixture mounted on top. The two BNL 32-channel ASICs are plugged into the bottom side of the board. The detector is kept in the fixture by the cap through which the high voltage is supplied to the cathode. The detector's anode side presses onto spring-loaded pogo pins making contact to the pads (see Fig. 2). The X-ray source (not shown in the figure) is placed centred above the detector's cap.

in one fabrication cycle.

2.2 Read-out system

Figure 3 shows the read-out system used to collect the signal from the fine-pitch detector. The detector is placed in the Ultem plastic fixture that is mounted on top of the adapter board. The gold-coated, spring-loaded pogo pins connect pixels with traces on a printed circuit board. The detector is kept in place with an Ultem cap. The cap is equipped with one pogo pin that is utilized to provide the high voltage to the cathode of the detector. The detector is read out by two 32-channel ASICs developed by G. De Geronimo (Brookhaven National Laboratory, BNL) and E. Wulf (Naval Research Laboratory, NRL).⁹ The adapter boards were designed at Washington University. Each channel is triggered by an adjustable threshold discriminator in the ASIC. The ASICs have a readout noise of around 2.5 keV FWHM. The ASIC channels were operated at a medium gain setting of 28.5 mV/fC and a signal shaping time of 0.5 μs .

The fine-pitch anode mask was designed in such a way that it can be read out by our current read-out system

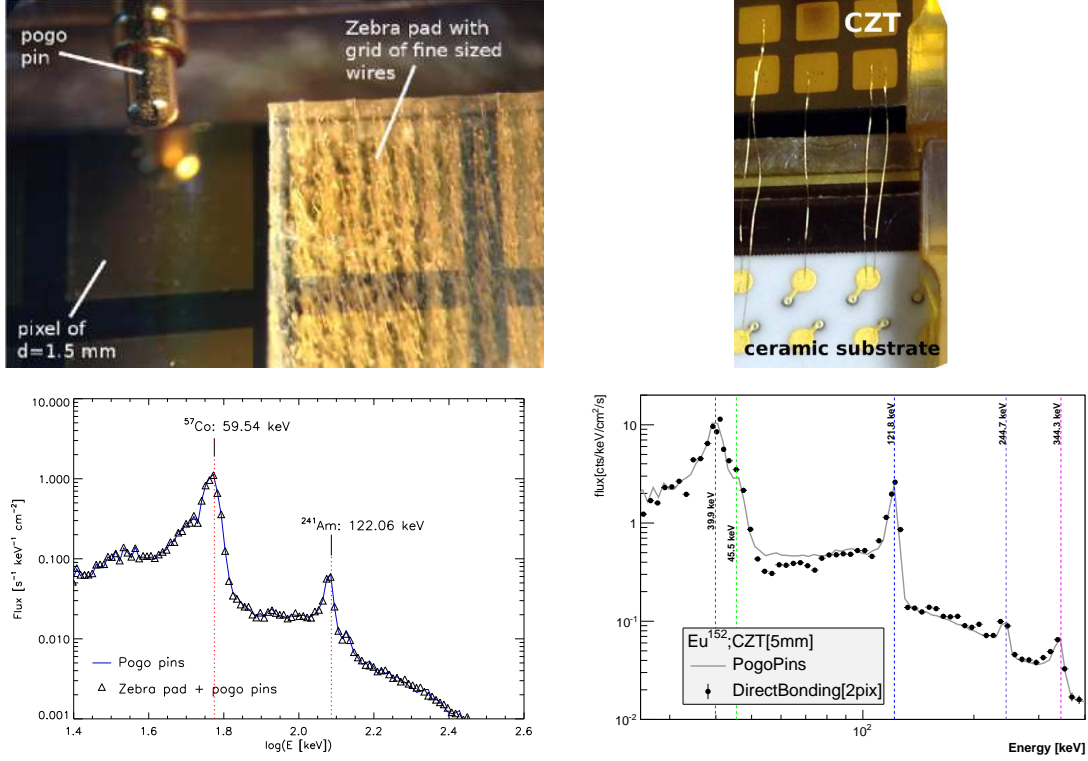


Figure 4. Different methods for transfer of signal from the detector's anodes to the read-out system: pixel/zebra pad/pogo pin combination (**top left**) and direct wire bonding between pixels and a ceramic adapter board (**top right**), which in turn is plugged into the ASIC board. Spectra obtained with each of the tested methods are presented in the bottom row. The **bottom left** panel shows data obtained with the system where the zebra pad was inserted between the detector and the pogo pins, while the **bottom right** panel shows measurements obtained from two wire-bonded pixels. In each case, the spectra are contrasted with the average detector spectrum obtained with our standard read-out method, i.e. pogo pins. ^{57}Co , ^{152}Eu and ^{241}Am radioactive sources were used in the tests. The presented tests of different options for signal transfer were carried out with a regular size 2.4 mm pixel pitch detector.

without the necessity of bump bonding the detector to the adapter board. This option offers a freedom in testing different anode designs simply by re-fabricating the detector surface. In a later step a detector with a full-sized fine-pitch anode will be fabricated and bump bonded for follow-up tests with a low noise small pixel ASIC (see Sec. 2.3).

The signal-transfer methods, in addition to the standard pogo pins, that are currently under consideration are zebra pad[†] placed between the pogo pins and the anode pads on the detector and direct gold wire bonds between the pixels and an ASIC/channel adapter board. The zebra pad would reduce the localized impact on the CZT crystal caused by a pogo pin point of contact. The direct wire bonding to pixels would simplify the detector fabrication and lead to lower resistance of the contact leads - if it can be applied successfully to fine pixel pitches. The two methods were tested on a detector purchased from Quikpak/Redlen[‡] with an anode of 8×8 pixels at 2.4 mm pitch and are illustrated in Fig. 4 (top). In the bottom row of Fig. 4 spectra obtained with each of the tested methods are presented. The energy calibrated spectra are also contrasted with the reference spectrum that was obtained with the system where only pogo pins were used to transfer the signal from pixels to

[†]Zebra pad is a silicon pad with a grid of fine-sized wires embedded into the pad. An example of zebra pad is shown in Fig. 4 (top left panel). By using a zebra pad we want to reduce the localized impact of pogo pins on the CZT crystal, and also on the thin metal/insulator layers of the sandwich-like structure of the small-sized anodes (i.e. prevent punching through the thin anode layers and shortening the contact pads to the grounded plate).

[‡]<http://redlen.ca>

ASIC channels. Though both, the zebra pad and the wire bonds, extend the travel path of the signal potentially exposing it to a pick up noise, no deterioration of spectral resolution and no increase of the noise component was observed in the obtained spectra. Thus, both signal-transfer methods can be used at the current stage of our project without any spurious effects being introduced into the collected data. The application of both approaches to pixels with pitches of $200\text{ }\mu\text{m}$ is currently being tested.

2.3 Development of a low noise, small pixel ASIC

To reduce the readout noise and to optimize the energy resolution and energy threshold of the individual pixels, it is advantageous to directly bond the readout ASIC to the detector pixels - with the ASIC/channel contact pads matched to the pixels of the detector. A number of ASICs with 2D pad arrays have been developed for CZT detectors with $350 - 600\text{ }\mu\text{m}$ pixel pitches. Our programme includes the design of the complete front-end channel of a 2D-ASIC (control logic and the physical layout), following the approach of ASIC designs for smaller-pixel-pitch detectors existing for Si-detectors.

A prototype front-end ASIC has been designed (Brookhaven National Laboratory) and fabricated in a commercial 130-nm process. The ASIC has a 16-by-16 channel array at the pitch of $250\text{ }\mu\text{m}$. Each channel includes a low-noise charge amplifier with adjustable gain, a shaper with baseline stabilizer at adjustable time constant (of peaking time 125, 250, 500, and 1000 ns), a discriminator, a peak-detector, and a 6-bit address register. Shared among channels are a pulse generator, bias circuits, global registers, and a low-voltage differential interface. Modes of operation are the following: acquisition, when events are detected and processed; readout, when events are read out in sparse mode with token passing; and configuration, when global and channel registers are accessible for configuration.

First tests of the ASIC are currently being performed. We plan to test the prototype of the newly developed ASIC next year, once the ASIC tests are finalized and the ASIC is directly bonded to a detector with a matching pixel grid. These developments will address the specific issues important for the use of the ASIC in X-ray astronomy: a low energy threshold and an excellent energy resolution.

2.4 Data analysis

Data presented in this paper were taken with either a ^{152}Eu radioactive source or the radioactive source combination of ^{57}Co and ^{241}Am . The ^{152}Eu source, with a half-life of 13.5 years, has emission lines at 39.8 keV, 121.8 keV, 244.7 keV and 344.3 keV. The ^{57}Co source, with a half-life of 271.8 days, shows emission lines at 14.4 keV, 122.1 keV and 136.5 keV. The ^{241}Am radioisotope has a half-life of 432.6 years and emission lines at 13.6 keV, 16.9 keV and 59.5 keV. During measurements the radioactive source was suspended on the cathode side approximately $1 - 2\text{ cm}$ above the detector's geometrical centre.

Energy calibration: Using a radioactive source placed above the detector, the energy scale of the individual pixels/channels was calibrated. In this step the fitted peak position of the emission lines in the raw uncalibrated spectrum is compared to the nominal energy of the selected lines in order to obtain the pedestal and amplification of each active ASIC channel. In the case where the detector was illuminated with ^{152}Eu , lines at 39.8 keV and 121.8 keV were used for calibration. The 59.5 keV line of ^{241}Am and 122.1 keV line of ^{57}Co were used for calibration when ^{241}Am and ^{57}Co were used in the measurements.

Characterisation of emission lines: The emission lines in the energy calibrated spectra were fitted with an asymmetric Gaussian function. The fitted profile allows for offsets and asymmetric widths σ_1 and σ_2 on the left and on the right side of the peak position in order to account for possible asymmetries in the line shapes. Whenever the ^{152}Eu source was used in the measurements, its low energy line at 39.8 keV was fitted with a profile consisting of a sum of two Gaussians. This fit accounts for the existence of the lower amplitude emission line at 45.7 keV, which at a few keV energy resolution is blended with the 39.8 keV line. Thus, if not taken into account, this line may cause systematic shifts in the fitted peak positions. The energy resolution is defined as the full width at half maximum FWHM of the fitted asymmetrical Gaussian function $\Delta E = \text{FWHM} = 2\sqrt{2\ln 2} \cdot \frac{1}{2}(\sigma_1 + \sigma_2)$. In the presented work the energy resolution is either given in units of keV or in relative units of $\Delta E/E$ (here E is the energy of the fitted emission line).

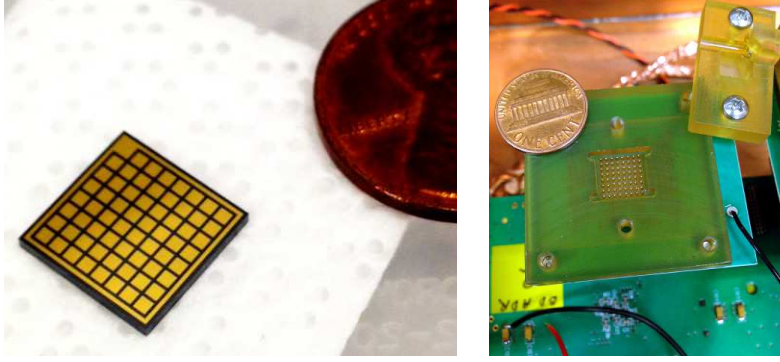


Figure 5. Acrorad CdTe detectors ($10 \times 10 \times 1 \text{ mm}^3$, pixel pitch 1.1 mm, pad size $0.88 \times 0.88 \text{ mm}^2$) with Pt cathode and Al/Ti/Au/Ni/Au pixels. **Left:** One of the five detectors as bought from Acrorad. **Right:** Ultem fixture and HV (designed and fabricated at Washington University), connected to the X-Calibur read-out system.^{6, 7}

3. RESULTS

3.1 Characterisation of CZT detectors with fine-pitch pixelated anode

A fine-pitch pixelated anode was successfully fabricated on a $20 \times 20 \times 5 \text{ mm}^3$ CZT detector (Fig. 2) purchased from Quikpak/Redlen. The detector was inserted into the existing read-out system, and the data are currently being taken. The ^{152}Eu radionuclide is used as a source of X-rays. The progress on the characterisation of the CZT detector with the fine-pitch pixelated anode will be reported at the SPIE 2014 conference.

3.2 Characterisation of thin CdTe detectors

Most detector backgrounds in space-missions scale with the volume of the detector crystal. This scaling leads to the choice of smaller detector thicknesses without compromising the X-ray absorption capabilities for $E \leq 100 \text{ keV}$. We therefore expanded our detector repository with five pixellated $10 \times 10 \times 1 \text{ mm}^3$ CdTe detectors (Fig. 6, left) bought from Acrorad[§]. We designed and fabricated a pogo pin fixture that matches the detectors with the smallest footprint and enables us to read them with our existing read-out infrastructure (Fig. 5, right). The CdTe detectors have monolithic platinum cathode. Their pixelated anode is made of Al/Ti/Au/Ni/Au thin metal layers and is comprised of 8×8 pixels with 1.1 mm pitch. The pixel grid is surrounded by a guard ring, which was set to ground throughout the measurements. All tests were performed with ^{152}Eu as the X-ray source with the detector/read-out system placed inside a temperature chamber.

In contrast to CZT detectors, CdTe detectors show an effect of increasing dark current with time. First, the steady growth of dark current with time is observed, then this growth is followed by an instantaneous increase in dark current level by an order of magnitude. This effect is referred to as a breakdown phenomenon.¹⁰ At higher temperatures, the dark current builds up more quickly until the point after which reliable measurements are no longer possible (in our case, starting after ~ 50 minutes at room temperature and after ~ 2.5 hours at -10°C). Therefore, operation at lower temperatures will guarantee a more stable and lengthier operation of the detectors.

Temperature tests of CdTe detectors: To test how the detector behaved at different temperatures, we analysed data from the detector biased to -300 V and operated at various temperatures (25°C , 17°C , 10°C , 0°C , -10°C , and -20°C). The trend of the energy resolution of the 40 keV peak for ^{152}Eu is shown in Fig. 6 (left). The boundaries of the band indicate the drift of resolution of the 40 keV peak with time. As displayed by the graph, the energy resolution worsens not only as the CdTe detector is at higher temperatures but also as this detector is working for longer[¶]. For each temperature, we optimized the ASIC channel trigger thresholds, which we found

[§]<http://www.acrorad.co.jp/us/>

[¶]Degradation of energy resolution with operation time observed for CdTe detectors is caused by a polarization effect.^{11, 12} When a bias voltage is applied and photon interaction occurs in the CdTe crystal, liberated electrons and holes travel towards their respective electrodes. In the presence of trapping sites, some of the charges can be trapped resulting in a reduction/modification of the internal electric field experienced by the carriers. The decrease of the electric

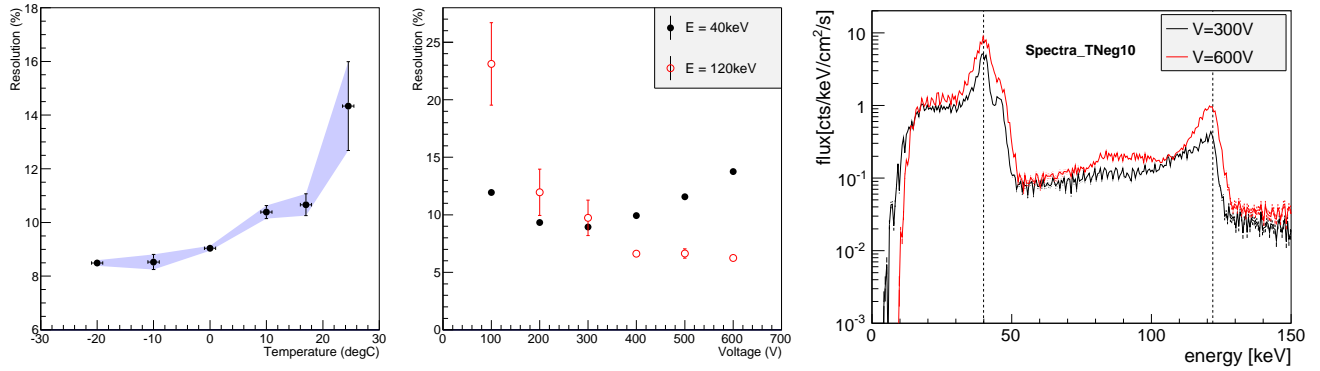


Figure 6. **Left:** energy resolution of the 40 keV energy line of ^{152}Eu as a function of temperature and as a function of time. The lower line of the band characterises the resolution after 10 minutes of data had been taken, while the upper line shows the resolution after 30 min (for $T = 10^\circ\text{C}$ and 17°C) or 50 min (for all other T). Note, however, that the detectors had been biased for 30 – 60 minutes prior to the start of the measurements (threshold optimization). **Middle:** resolution of the 40 keV and 120 keV energy lines of ^{152}Eu as a function of bias voltage. The data points result from 80-minute data runs. **Right:** energy spectra of ^{152}Eu measured at two different voltages at $T = -10^\circ\text{C}$.

we must increase more at temperatures lower than -10°C (the thresholds were found to be around 15 keV). From this factor, in combination with the resolution graph, we concluded that of the temperatures we tested, -10°C is the optimal temperature at which to run the CdTe detector.

Bias voltage dependence of energy resolution for CdTe: Given that we determined -10°C to be the optimal temperature at which to use the CdTe detector, we kept our system in this environment as we tested different bias voltages (-50 V , -100 V , -200 V , -300 V , -400 V , -500 V , and -600 V). As Figure 6 (middle) displays, the trends of energy resolution vs. bias voltage differ according to the peak studied. For the 40 keV peak of ^{152}Eu , -300 V is the optimum for resolution. At -50 V , the 40 keV line is no longer well-defined (merging with the threshold regime). For the 120 keV peak, however, the resolution improves at higher voltages, beginning to level off after -500 V . Figure 6 (right) shows this difference in resolution at -300 V and -600 V . The -600 V provides better resolution at the high energy lines. We are currently testing 4 other $10 \times 10 \times 1\text{ mm}^3$ CdTe detectors. These detectors will also be used in the long-term to test sub-mm pixel pitches.

We also bought two $20 \times 20 \times 1.2\text{ mm}^3$ CdTe crystals from Acrorad and fabricated detectors with a Au cathode and In/Ti/Au pixels (Fig. 7, bottom). I/V curves of the detectors were taken and energy spectra were recorded at different temperatures and with different radioactive isotopes. We find excellent performance (measured at $T = -30^\circ\text{C}$) with all-pixel averaged energy resolutions of $3.2 \pm 0.1\text{ keV}$ (8.1%) at 40 keV (Fig 7, top left), $3.2 \pm 0.3\text{ keV}$ ($5.4 \pm 0.4\%$) at 59.5 keV and $5.3 \pm 0.3\text{ keV}$ ($4.3 \pm 0.2\%$) at 121.8 keV. Note, that the ^{152}Eu 40 keV line actually consists of two close-by lines at 39.5 keV and 40.1 keV. Furthermore, we resolve the 14 keV line of ^{57}Co corresponding to the lowest energy threshold of around 10 keV achieved in our group so far (see Fig. 7, top right).

4. SUMMARY

In the presented paper we reported on our progress in the development and testing of X-ray detectors with fine-pitch pixelated anode. We designed a small-pixel photomask consisting of pixel blocks with different pixel dimensions and pixel pitches. The investigated pixel pitch range and pixel size range are: $200 - 500\text{ }\mu\text{m}$, and $100 - 250\text{ }\mu\text{m}$, respectively. The first detector, made of CZT, with small-pixel blocks has been fabricated and is

field reduces drift velocities of the charges and in turn more carriers are being trapped. This polarization effect causes a decrease in counting rate and pulse amplitude with time. It is important to mention that this effect is most severe when operating at high temperatures and low bias voltages.

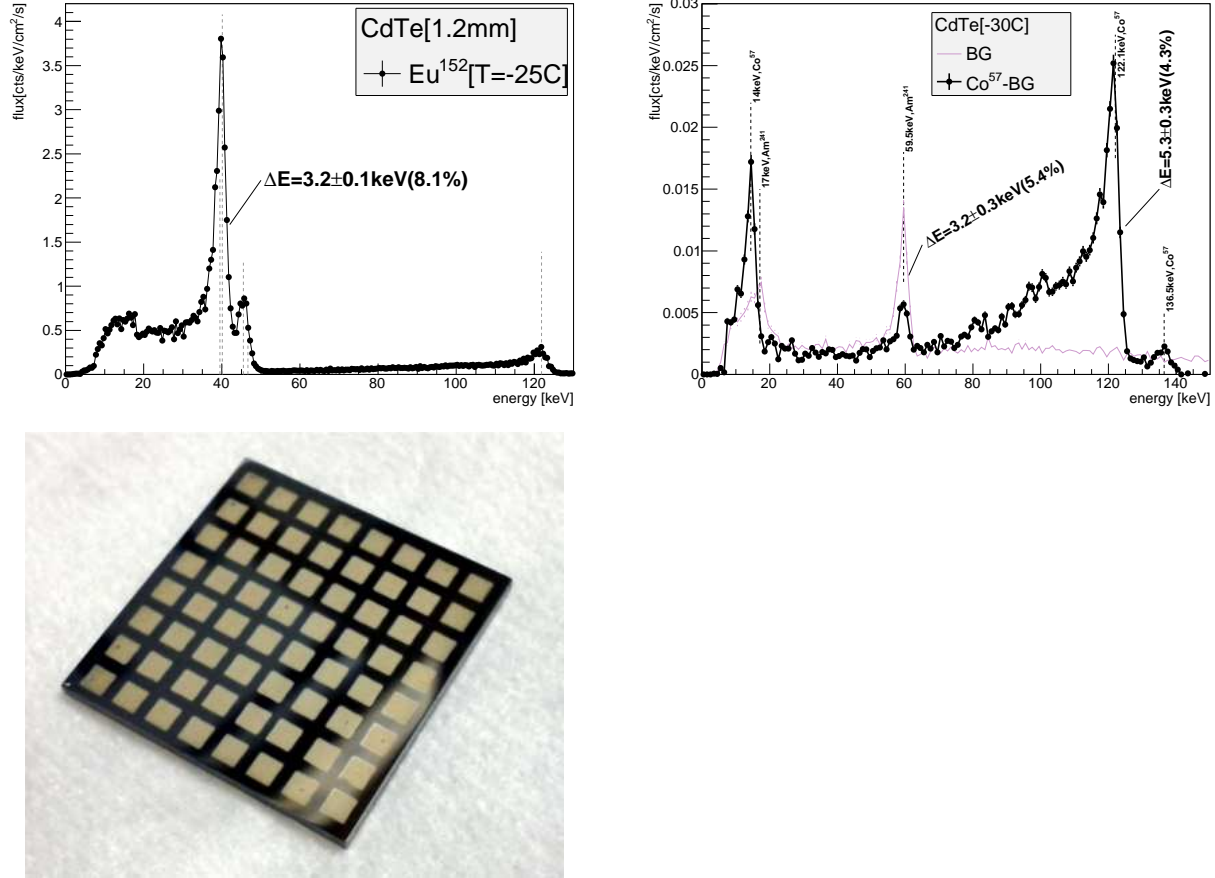


Figure 7. CdTe detector ($20 \times 20 \times 1.2 \text{ mm}^3$, substrate from Acrorad). **Bottom left:** Detector fabricated at Washington University with Au cathode and In/Ti/Au pixels. **Top left:** Energy spectrum measured with ^{152}Eu ($T = -25^\circ\text{C}$ and bias voltage of -400 V) with excellent energy resolution. The vertical lines indicate the nominal line energies (relative heights represent emission intensities times photo-absorption probability in 1.2 mm of CdTe). **Top right:** Energy spectrum measured with a (weak) ^{57}Co source ($T = -30^\circ\text{C}$ and bias voltage of -400 V). The background spectrum with lines at 17 keV and 59.5 keV is a likely result of an ^{241}Am smoke detector installed in the temperature chamber. The ^{57}Co line at 14 keV can be resolved.

currently being tested. The progress of the performance study of the fine-pitch pixelated CZT detector will be reported at the SPIE 2014 conference.

Different methods of contacting pixels to the readout ASIC were considered (pogo pins, zebra pads, direct wire bonding) and successfully tested on pixelated anodes with 2.4 mm pixel pitch. Currently, we are in the process of testing how these methods can be applied to fine-pitch pixels.

We also characterised 1 mm thin CdTe detectors. We studied their performance at different temperatures. The optimal temperature, yielding best performance in terms of energy resolution but also dark current stability, was determined. The studied CdTe detectors show excellent energy resolution of $\sim 8\%$ at 40 keV.

ACKNOWLEDGMENTS

We are grateful for NASA funding from grant NNX13AC49G.

REFERENCES

- [1] Zhang, W. W., Biskach, M. P., Blake, P. N., Chan, K. W., Evans, T. C., Hong, M. L., Jones, W. D., Kolos, L. D., Mazzarella, J. M., McClelland, R. S., O'Dell, S. L., Saha, T. T., and Sharpe, M. V., "Lightweight and high angular resolution x-ray optics for astronomical missions," in [*Society of Photo-Optical Instrumentation Engineers (SPIE) Conference Series*], *Society of Photo-Optical Instrumentation Engineers (SPIE) Conference Series* **8147** (Sept. 2011).
- [2] Ramsey, B., Kilaru, K., Gubarev, M., Gaskin, J., O'Dell, S., Kolodziejczak, J., Romaine, S., Zhang, W., and Atkins, C., "Improving X-Ray Optics Through Differential Deposition," in [*response to NASA solicitation NNH11ZDA018L (Enabling Technology)*], <http://pcos.gsfc.nasa.gov/studies/rfi/Ramsey-Brian-RFI.pdf> (2011).
- [3] Limousin, O., "New trends in CdTe and CdZnTe detectors for X- and gamma-ray applications," *Nuclear Instruments and Methods in Physics Research A* **504**, 24–37 (May 2003).
- [4] Takahashi, T. and Watanabe, S., "Recent progress in CdTe and CdZnTe detectors," *IEEE Transactions on Nuclear Science* **48**, 950–959 (Aug. 2001).
- [5] Barthelmy, S. D., "Burst Alert Telescope (BAT) on the Swift MIDEX mission," in [*X-Ray and Gamma-Ray Instrumentation for Astronomy XIII*], Flanagan, K. A. and Siegmund, O. H. W., eds., *Society of Photo-Optical Instrumentation Engineers (SPIE) Conference Series* **5165**, 175–189 (Feb. 2004).
- [6] Beilicke, M. G., Baring, M., Barthelmy, S., Binns, W. R., Buckley, J., Cowsik, R., Dowkontt, P., Garson, A., Guo, Q., Haba, Y., Israel, M. H., Kislat, F., Kunieda, H., Lee, K., Martin, J., Matsumoto, H., Miyazawa, T., Okajima, T., Schnittman, J., Tamura, K., Tueller, J., and Krawczynski, H., "The Hard X-ray Polarimeter X-Calibur: Astrophysical Motivation and Performance," *SPIE* **8507**, 85071 (2012).
- [7] Beilicke, M., Kislat, F., Zajczyk, A., Guo, Q., Endsley, R., Stork, M., Cowsik, R., Dowkontt, P., Barthelmy, S., Hams, T., Okajima, T., Sasaki, M., Zeiger, B., De Geronimo, G., Baring, M. G., and Krawczynski, H., "Design and tests of the hard X-ray polarimeter X-Calibur," *The Journal of Astronomical Instrumentation* **submitted**.
- [8] Li, Q., Beilicke, M., Lee, K., Garson, A., Guo, Q., Martin, J., Yin, Y., Dowkontt, P., De Geronimo, G., Jung, I., and Krawczynski, H., "Study of thick CZT detectors for X-ray and Gamma-ray astronomy," *Astroparticle Physics* **34**, 769–777 (May 2011).
- [9] Wulf, E. A., Philips, B. F., Neil Johnson, W., Kurfess, J. D., Novikova, E. I., O'Connor, P., and De Geronimo, G., "Compton imager for detection of special nuclear material," *Nuclear Instruments and Methods in Physics Research A* **579**, 371–374 (Aug. 2007).
- [10] Garson, III, A. B., Jung, I. V., Perkins, J., and Krawczynski, H., "Evaluation of 5 mm-thick CdTe Detectors from the Company Acrorad," *ArXiv Astrophysics e-prints* (Nov. 2005).
- [11] Bell, R. O., Entine, G., and Serreze, H. B., "Time-dependent polarization of CdTe gamma-ray detectors," *Nuclear Instruments and Methods* **117**, 267–271 (May 1974).
- [12] Cola, A. and Farella, I., "The polarization mechanism in CdTe Schottky detectors," *Applied Physics Letters* **94**, 102113 (Mar. 2009).